Title :
ORCHIDEE MICT-LEAK (r5459), a global model for the production, transport and transformation of dissolved organic carbon from Arctic permafrost regions, Part 2: Model evaluation over the Lena River basin.

Authors:
S.P.K. Bowring[1], R. Lauerwald[2], B. Guenet[1], D. Zhu[1], M. Guimberteau[1,3], P. Regnier[2], A. Tootchi[3], A. Ducharne[3], P. Ciais[1]

Affiliations:
[1] Laboratoire des Sciences du Climat et de l'Environnement, LSCE, CEA, CNRS, UVSQ, 91191 Gif Sur Yvette, France
[2] Department of Geoscience, Environment & Society, Université Libre de Bruxelles, Bruxelles, Belgium
[3] Sorbonne Université, CNRS, EPHE, Milieux environnementaux, transferts et interaction dans les hydrosystèmes et les sols, Metis, 75005 Paris, France

Abstract
In this second part of a two-part study, we perform a simulation of the carbon and water budget of the Lena catchment with the land surface model ORCHIDEE MICT-LEAK, enabled to simulate dissolved organic carbon (DOC) production in soils and its transport and fate in high latitudes inland waters. The model results are evaluated in their ability to reproduce the fluxes of DOC and carbon dioxide (CO_2) along the soil-inland water continuum, and the exchange of CO_2 with the atmosphere, including the evasion outgassing of CO_2 from inland waters. We present simulation results over years 1901-2007, and show that the model is able to broadly reproduce observed state variables and their emergent properties across a range of interacting physical and biogeochemical processes, including: 1) Net primary production (NPP), respiration and riverine hydrologic amplitude, seasonality and inter-annual variation; 2) DOC concentrations, bulk annual flow and their volumetric attribution at the sub-catchment level; 3) High headwater versus downstream CO_2 evasion, an emergent phenomenon consistent with observations over a spectrum of high latitude observational studies. (4) These quantities obey emergent relationships with environmental variables like air temperature and topographic slope that have been described in the literature. This gives us confidence in reporting the following additional findings: Of the ~34TgC yr^{-1} left over as input to soil matter after NPP is diminished by heterotrophic respiration, 7 TgC yr^{-1} is leached and transported into the aquatic system. Of this, over half (3.6 TgC yr^{-1}) is evaded from the inland water surface back into the atmosphere and the remainder (3.4 TgC yr^{-1}) flushed out into the Arctic Ocean, mirroring empirically derived studies. These riverine DOC exports represent ~1.5% of NPP. DOC exported from the floodplains is dominantly sourced from recent, more 'labile' terrestrial production, in contrast to DOC leached from the rest of the watershed with runoff and drainage, which is mostly sourced from recalcitrant soil and litter. All else equal, both historical climate change (a spring/summer warming of 1.8°C over the catchment) and rising atmospheric CO_2 (+85.6ppm) are diagnosed from factorial simulations to contribute similar, significant increases in DOC transport via primary production, although this similarity may not hold in the future.

1 Introduction

A new branch of the high latitude-specific land surface component of the IPSL Earth System model, ORCHIDEE MICT-LEAK (r5459), was enabled to simulate new model processes of soil dissolved organic carbon (DOC) and CO_2 production, and their advective/diffusive vertical transport within a discretized soil column as well as their transport and transformation within the inland water network, in addition to improved representation of hydrological and carbon processes in floodplains. These additions, processes first coded in the model ORCHILEAK (Lauerwald et al., 2017) and implemented within the high latitude base model ORCHIDEE-MICT v8.4.1 (Guimberteau et al., 2018), were described in detail in Part 1 of this study, depicted graphically in Figure S1a,b. This second part of our study deals with the validation and application of our model. We validate simulation outputs against observation for present-day and run transient simulations over the historial period (1901-2007) using the Lena River basin as test case. The simulation setup and rationale for choice of simulation basin are outlined below.

2 Simulation Rationale

The Lena river basin, which is bounded by the region 52-72°N; 102-142°E, was chosen as the basin for model evaluation because it is the largest DOC discharge contribution amongst the Arctic rivers, according to some estimates (Raymond et al., 2007; Holmes et al., 2012), with its 2.5 million km^2 area (befitting our coarse-grid resolution) discharging almost 20% of the summed discharge of the largest six Arctic rivers, its large areal coverage by Podzols (DeLuca and Boisvenue, 2012), and the dominance of DOC versus particulate organic carbon (POC) with 3-6Tg DOC-C yr^{-1} vs. 0.03-0.04 Tg POC-C yr^{-1} (Semiletov et al., 2011) in the total OC discharge load –factors all broadly representative of the Eurasian Arctic rivers. Climatological input to the model is from the Global Soil Wetness Project Phase 3 (GSWP3) v.0 data, based on 20th Century reanalysis using the NCEP land-atmosphere model and downscaled to a 0.5°, 3-hourly resolution covering the period 1901 to 2007 (Supplement, Table S1). This is then upscaled to 1° resolution and interpolated to a 30 minute timestep to comply with the timestep of ORCHIDEE's surface water and energy balance calculation period. Precipitation was partitioned into rainfall and snowfall, and a correction for wind-induced undercatch was also applied. These are described in greater detail in Guimberteau et al. (2018). Over the simulation period under this dataset, the Lena basin experiences a mean thaw period warming of 1.8°C, while atmospheric CO_2 concentrations increase by 85.6ppm. The GSWP3 dataset was chosen due to its relative performance in simulating the inter-annual variability and seasonality of Pan-Arctic riverine discharge in ORCHIDEE-MICT (Guimberteau et al., 2018), as compared to another data-driven climate forcing product, CRUNCEP v7 (Kalnay et al., 1996; New et al., 1999). Indeed, under CRUNCEP v7, ORCHIDEE-MICT was shown to underestimate river discharge by as much as 83% over the Yukon basin. An improved floodplains area input file for the Lena basin (Tootchi et al., 2019) was used to drive the simulation of floodplain dynamics (Supplement, Table S1).

3 Simulation Setup

As detailed in Part 1 (Section 3.1), the soil carbon stock used by our model was reconstituted from a 20,000 year soil carbon spinup of an ORCHIDEE-MICT run from

98   Guimberteau et al. (2018) and run to quasi-steady state equilibrium for the Active and
99   Slow carbon pools (Supplement, Fig. S1b) under the new soil carbon scheme used in the
100 model configuration of the present study (Fig. 1). After some adjustment runs to account
101 for model read/write norms, the model was then run in transient mode under historical
102 climate, land cover and atmospheric CO_2 concentrations (Fig. 1). Simulations were run
103 over the Lena river basin (Fig. 3a) for the climate, CO_2 and vegetation input forcing data
104 (Supplement, Table S1) over 1901-2007 at a 1 degree resolution (Fig. 1), to evaluate the
105 simulated output of relevant carbon fluxes and hydrologic variables against their
106 observed values, as well as those of emergent phenomena arising from their interplay
107 (Fig. 1). We evaluate at the basin scale because the isolation of a single geographic unit
108 allows for a more refined analysis of simulated variables than doing the same over the
109 global Pan-Arctic, much of which remains poorly accounted for in empirical databases
110 and literature.   The literature studies used in this evaluation are summarised in Table
111 S2. In order to derive an understanding of the environmental drivers of carbon cycling in
112 the Lena watershed and analyse the model sensitivity to the corresponding forcing data,
113 alternative simulations were run with constant climate and CO_2 conditions (Table 1, and
114 Supplement Table S1). Thus a factorial simulation was devised, consisting of 2 factors
115 and 3 simulations whose inputs were otherwise identical but for the investigated factor
116 (Table 1).
117
118
119 **4 Results and Interpretation**
120
121 We refer to different simulations performed in this study according to the sensitivity
122 factors to which they are subjected. The transient, historical climate and atmospheric
123 CO_2 -forced simulations are hereafter referred to as the "Control" (CTRL) scenario, for
124 ease of interpretation . The "CLIM" and "CO_2" scenarios are those simulations for which
125 climate variability and atmospheric CO_2 were held constant at their pre-industrial levels,
126 respectively (Table 1). The following evaluation sections compare observations solely
127 against the CTRL. The subsequent section will evaluate this comparison against the
128 factorial simulations described above. The overall carbon budgets and their fluxes as
129 generated by each of the simulations are shown in Figs. 2 and 11 and discussed in detail
130 at the end of the evaluation. In the following we report first the broad results of model
131 simulations with respect to the carbon cycle, and follow with an evaluation of river
132 water and DOC discharge, DOC concentration and seasonality and river surface CO_2
133 outgassing, against available empirical data. Evaluation of NPP and Soil Respiration,
134 which are not considered primary to this study, is covered in Supplementary Text S1.
135 **4.1 Model Output: Carbon Budget**
136
137 Fig. 2 summarises the simulated components of the carbon (C) cycle across the Lena
138 basin, averaged over the decade 1998-2007. C inputs to terrestrial ecosystems are
139 dominated by photosynthetic input (GPP). GPP assimilates (875 TgC yr^{-1}) are either
140 used as metabolic substrate by plants and lost as CO_2 by plant respiration processes
141 (376 TgC yr^{-1}) or soil respiration processes (465 TgC yr^{-1}), leaving behind annual growth
142 in terrestrial C storage (net biome productivity (NBP)), an atmospheric CO_2 sink of 34
143 TgC yr^{-1}. Further C inputs are delivered to the terrestrial surface via a combination of
144 atmospheric deposition, rainwater dissolved C, and the leaching of canopy C
145 compounds. These sum to a flux transported to the soil surface (4.6 TgC yr^{-1}) by
146 throughfall (see Part 1, Section 2.5).

147

148 DOC in the soil solution as well as a fraction of dissolved CO_2 produced in the root zone
149 from root and microbial respiration is exported to rivers along the model's two
150 hydrological export vectors, surface runoff and deep drainage (Part 1, Section 2.6). For
151 the Lena basin simulations, these fluxes of C exported from soils amount to 5.1 and 0.2
152 $TgC\ yr^{-1}$, for DOC and CO_2 respectively. Three water pools, representing streams, rivers
153 and groundwater and each containing dissolved CO_2 and well as DOC of different
154 reactivity, are routed through the landscape and between grid cells following the river
155 network in the catchment (Part 1, Section 2.7). In addition, seasonally flooded soils
156 located in low, flat grid cells next to the river network (see Part 1, Section 2.8) export
157 DOC (0.57 $TgC\ yr^{-1}$) and CO_2 (1.54 $TgC\ yr^{-1}$) to the river network when their inundation
158 occurs. Part of this leached inundated material is re-infiltrated back into the soil from
159 the water column during floodplain recession ('Return' flux, 0.45 $TgC\ yr^{-1}$). During its
160 transport through inland waters, DOC can be decomposed into CO_2 (2.1 $TgC\ yr^{-1}$) and a
161 fraction of river CO_2 produced from DOC and transferred from soil escapes to the
162 atmosphere (3.6$TgC\ yr^{-1}$) through gas exchange kinetics (Part 1, Section 2.10). This flux
163 is termed 'CO_2 evasion' in Fig. 2 of this study. Carbon that survives the inland water
164 reactor is exported to the coastal ocean in the form of DOC (3.16 $TgC\ yr^{-1}$) and CO_2 (0.26
165 $TgC\ yr^{-1}$).

166

167 **4.2.1 Model Evaluation: River Discharge**

168

169 Simulated river water discharge captures the key feature of Arctic river discharge – that
170 of a massive increase in flow to $\sim$80,000 m^3s^{-1} in April-June caused by melting snow and
171 ice, but underestimates observed river discharge in late summer by around 70% (Figs.
172 3c, 4b). In addition, the mean spring (June) discharge peak flows are slightly
173 underestimated or out of phase in simulations (Figs. 3c, 4b) compared to observations
174 (Ye et al., 2009): this is caused by a large amount of water throughput being simulated in
175 May ($\sim$10,000 $m^3\ s^{-1}$) in excess of observed rates. Finally, during the winter low-flow
176 period, the model consistently under-estimates water flow-through volumes reaching
177 the river main stem (see Fig. 3c, winter months). Although this underestimate is not
178 severe relative to annual bulk flows, the divergence is large as a percentage of
179 observations (see right-hand axis, Fig. 3c), and may point to an issue in how ice is
180 represented in the model, such as the fact that solid ice inclusions in the soil column are
181 not represented, or the possibility that much slower groundwater dynamics than those
182 represented in the model are feeding discharge. In addition to this, the presence of a
183 dam on the Vilui tributary of the Lena has been shown to reduce main stem winter low-
184 flow rates by up to 90% (Ye et al., 2003), similar to the discrepancy of our low-flow
185 rates: given that our model only simulates 'natural' hydrological flows and thus does not
186 include dams, we expect that this effect is also at play. Causal factors for the apparently
187 poor performance of the hydrological module range from poor model representations
188 (or lack thereof), climatological dataset choices and deficiencies in evaluation datasets
189 themselves, and are covered in detail in the Supplement (Text S2).

190

191 **4.2.2 Model Evaluation: DOC Annual Discharge**

192

193 Our CTRL simulation shows that the yearly sum of DOC output to the Arctic Ocean has
194 increased steadily over course of the 20th Century, from $\sim$1.4Tg DOC-C yr^{-1} in 1901 to
195 $\sim$4Tg DOC-C yr^{-1} in 2007 (Fig. 4a). Smoothing the DOC discharge over a 30-year

196 running mean shows that the increasing trend (Fig. 4a) over this averaging scale is
197 almost linear, at ~0.11TgC per decade, or a net increase of 40% using this averaging
198 scale. Empirically based estimates of total contemporary DOC entering the Laptev Sea
199 from Lena river discharge vary around ~2.5-5.8 TgC-DOC (Cauwet and Sidorov, 1996;
200 Dolman et al., 2012; Holmes et al., 2012; Lara et al., 1998; Raymond et al., 2007;
201 Semiletov et al., 2011).
202
203 Note however that modelled aggregate DOC discharge is strongly affected by the
204 underestimation of river water discharge. Fig. 4a shows the average simulated DOC
205 discharge (red bar) of the last decade (1998-2007) of 3.2 TgC yr^{-1}, to be compared with
206 estimates of 3.6 TgC yr^{-1} (black bar) from Lara et al. (1998) and 5.8 TgC yr^{-1} (orange bar)
207 from Raymond et al. (2007) and 5.7 TgC yr^{-1} from Holmes et al. (2012). The most recent
208 and elaborate of those estimates is that of Holmes et al. (2012) who used a rating curve
209 approach based on 17 samples collected from 2003 to 2006 and covering the full
210 seasonal cycle, which was then applied to 10 years of daily discharge data (1999-2008)
211 for extrapolation. Given that their estimate is also based on Arctic-GRO-1/PARTNERS
212 data (https://www.arcticgreatrivers.org/data), which stands as the highest temporal
213 resolution dataset to date, their estimate is likely the most accurate of the DOC discharge
214 estimates. Compared to their average annual estimate of 5.7 TgC yr^{-1}, our simulated
215 DOC export is low by around 43%, due largely to the poor performance of the hydrology
216 module. The DOC discharge underestimate is discussed in depth in Supplement (Text
217 S2).
218
219
220 **4.3 Model Evaluation: DOC Concentrations in lateral transport**
221
222 While total DOC discharge captures the integral of biogeochemical processes leading tha
223 fluvial outflow, simulations of this are highly sensitive to the performance of modelled
224 hydrology and climatological input data. A more precise measure for the performance
225 of the newly-introduced DOC production and transport module, which is less sensitive
226 to reproduction of river water discharge, is DOC concentration. This is because while
227 the total amount of DOC entering river water depends on the amount of water available
228 as a vehicle for this flux (hydrology), the concentration of DOC depends on the rate of
229 soil carbon leaching, itself depending largely on the interaction of soil biogeochemistry
230 with primary production and climatic factors. This we evaluate in Figure 5a, This shows
231 that for the majority of the thaw period or growing season (April-September), which
232 corresponds to the period during which over 90% of DOC production and transport
233 occurs, the model largely tracks the observed seasonality of DOC concentrations in
234 Arctic-GRO data averaged over 1999-2007. There is a large overestimate of the DOC
235 concentration in May owing to inaccuracies in simulating the onset of the thaw period,
236 while the months June-September underestimate concentrations by an average of 18%.
237 On the other hand, frozen period (November-April) DOC concentrations are
238 underestimated by between ~30-500%. This is due to deficiencies in representing
239 wintertime soil hydrological water flow in the model, which impedes water flow when
240 the soil is frozen, as discussed in Section S2. Because of this deficiency, slow-moving
241 groundwater flows that contain large amounts of DOC leachate are under-represented.
242 This interpretation is supported by the fact that in both observations and simulations, at
243 low discharge rates (corresponding to wintertime), DOC concentrations exhibit a strong
244 positive correlation with river discharge, while this relationship becomes insignificant at

245 higher levels of river discharge (Fig. 5b). Thus wintertime DOC concentrations suffer
246 from the same deficiencies in model representation as those for water discharge.   In
247 other words, the standalone representation of DOC leaching is satisfactory, while when
248 it is sensitive to river discharge, it suffers from the same shortfalls identified in Sections
249 S2 and S3. Modelled DOC concentrations in stream, river and ground water are
250 evaluated against data and discussed in the Supplement (Text S5).
251
252 **4.4 In-Stream CO_2 Production, Transport, Evasion**
253
254 In our model, the fate of DOC once it enters the fluvial system is either to remain as DOC
255 and be exported to the ocean, or to be degraded to dissolved CO_2 ($CO_{2(aq.)}$), which is
256 itself either also transported to the marine system or outgassed from the fluvial surface
257 to the atmosphere (see Part 1, Section 2.10 and Text S6). As noted in Part 1 of this study,
258 although the model as a whole conducts simulations at the 1 degree scale, the routing of
259 water and carbon, as well as the evasion of the latter, occurs at the sub-grid scale, such
260 that we are able to simulate spatially explicit rivers whose size approximates Strahler
261 order 4, and through the 'fast' water pool in the model are able to simulate streams of
262 Strahler order 1-3.   The seasonality of riverine dissolved CO_2 concentrations ($CO_{2(aq.)}$,
263 mgC L^{-1}) is evaluated in Fig. 4c to compare $CO_{2(aq.)}$ concentrations with DOC bulk flows,
264 since $CO_{2(aq.)}$ concentrations follow an inverse seasonal pattern to those of DOC, being
265 highest during the winter baseflow period and lowest in summer due to dilution during
266 its high discharge phase (Semiletov et al., 2011). The simulated flow of $CO_{2(aq.)}$ at Kusur
267 (Fig. 4c, dashed red) reproduces the seasonality of observations from Cauwet and
268 Sidorov (1996), who sampled the Lower Lena (Fig. 3a), but somewhat underestimates
269 concentrations. Also included in Fig. 4c is the basin average for all non-zero values,
270 whose shape also tracks that of observations. Thus the model represents on the one
271 hand increasing hydrological flow mobilising increasing quantities and concentrations
272 of DOC while on the other hand those same increasing hydrological flows increasing the
273 flux, but decreasing the concentration, of $CO_{2(aq.)}$ throughput.
274
275 Evaluation of modelled CO_2 evasion is beset by problems, not least that no data on this
276 quantity have to our knowledge been recorded for the Lena (see Text S6). Figure 6
277 summarises some of the results from the simulated water body CO_2 outgassing flux.
278 Year-on-year variation in basin-wide evasion from river, stream and floodplain sources
279 combined exhibits a marked increasing trend over the course of the 20th Century,
280 increasing from a minimum of ~1.6 $TgCO_2$-C yr^{-1} in 1901 to a maximum of ~4.4 $TgCO_2$-C
281 yr^{-1} in 2007 (+300%, Fig. 7a). Smoothing the data over a 30 year running average yields
282 a dampened net increase in basin-wide evasion of ~30% (Fig. 7a). Thus yearly evasion
283 flux is some 105% of yearly DOC discharge to the coast from the Lena basin and 51% of
284 C exported from soils to headwaters as CO_2 or DOC. If we compare the mean yearly rate
285 of increase in absolute (TgC yr^{-1}) CO_2 evasion and DOC discharge based on linear
286 regression over the whole simulation period, it appears that the rate of increase of both
287 fluxes has been strikingly similar over the simulated 20th Century, with mean increases
288 of 11.1 GgC yr^{-1} and 11.5 GgC yr^{-1} per year for evasion and export, respectively. A
289 summary and evaluation of the source and seasonal heterogeneity of evasion is
290 discussed in the Text S7.
291
292
293 As previously discussed, the proportion of total basin-wide CO_2 evasion attributable to

294　headwater streams and rivers is substantially greater than their proportion of total
295　basin surface area. Figure 6b represents the mean monthly fractional contribution of
296　each surface hydrological water pool to the total evasion flux (unitless) over the period
297　1998-2007. This shows that over the entirety of the thaw period, the stream water pool
298　takes over from the river water pool as the dominant evasion source, particularly at the
299　height of the freshet period, where its fractional contribution rises to >75%. The stream
300　fraction of August outgassing is ~57% of the annual total, which is higher than the
301　~40% found for streams in Denfeld et al. (2013). However, the values between the two
302　studies are not directly comparable, different basins notwithstanding, due to differences
303　between how 'streams' are defined in the model and in the field (expanded on in Text
304　S8). Also shown in Fig. 6b is the gradual onset of evasion from the floodplain reservoir in
305　April, as the meltwater driven surge in river outflow leads to soil inundation and the
306　gradual increase of proportional evasion from these flooded areas over the course of the
307　summer, with peaks in June-August as water temperatures over these flooded areas
308　likewise peak. We stress the importance of these simulation results as they concur with
309　large numbers of observational studies (cited above) which show smaller headwater
310　streams' disproportionately large contribution to total outgassing (Fig. 7c), this being
311　due to their comparatively high outgassing rates (Fig. 7e). In addition, the contribution
312　of floodplains to evasion, an otherwise rarely studied feature of high latitude biomes, is
313　shown here to be significant. A Hovmöller plot (Fig. 7d) of the monthly longitude-
314　averaged stream reservoir fraction of total evasion, allows us to infer that: (i) The
315　dominance of stream evasion begins in the most southern upstream headwaters in the
316　lower latitude thaw period (April-May), and trickles northward over the course of the
317　next two months, following the riverflow. (ii) The intensity of this evasion is greatest in
318　the lower latitude regions of the basin, which we speculate is the result of higher
319　temperatures causing a greater proliferation of small thaw water-driven flows and
320　evasion. (iii) Areas where the stream fraction is not dominant or only briefly dominant
321　during the summer (58-60°N, 63-64°N, 70-71°N) are all areas where floodplain CO_2
322　evasion plays a prominent role at that latitudinal band.
323
324　We evaluate the approximate rate of modelled areal CO_2 efflux from the water surface
325　against observations from Denfeld et al. (2013). (The 'approximate' caveat is treated in
326　the Supplementary Text S9). The comparison of simulated results with those from
327　Denfeld et al. (2013) are displayed in Fig. 6d, which shows boxplots for simulated CO_2
328　evasion from the stream water reservoir and river water reservoir averaged over 1998-
329　2007. The empirical (Kolyma river) analogue of this data, from which this plot is
330　inspired (Fig. 4d in Denfeld et al., 2013), is shown in inset. Median efflux was 1.1 (6)
331　versus 0.4 (0.8) for stream and river, respectively, in simulations (observations). Like
332　the observations, simulated stream efflux had a substantially greater interquartile range,
333　mean (24.6) and standard deviation (73) than total river efflux (1.3 and 7.2,
334　respectively).
335
336　**4.5.Emergent Phenomena: DOC and topographic slope, MAAT**
337
338　Subsurface water infiltration fluxes and transformations of dissolved matter represent
339　an important, if poorly understood and observationally under-represented
340　biogeochemical pathway of DOC export to river main stems, involving the complex
341　interplay of slope, parent material, temperature, permafrost material age and soil
342　physical-chemical processes, such as adsorption and priming. In the Lena basin, as in

other permafrost catchments, topographic slope has been shown to be a powerful predictor for water infiltration depth, and concentration and age of DOC (Jasechko et al., 2016; Kutscher et al., 2017; McGuire et al., 2005), with deeper flow paths and older, lower DOC-concentrated waters found as the topographic slope increases. This relationship was shown in Fig. 4 of Kutscher et al. (2017) who surveyed DOC concentrations across a broad range of slope angle values in the Lena basin and found a distinct negative relationship between the two. Comparing the Kutscher et al. (2017) values with our model output, by plotting stream and river DOC concentrations averaged per gridpoint over 1998-2007 against the topographic map used in the routing scheme (Fig. 8) we find a similar negative relationship between the two variables. The causes of this relationship and a discussion of the model's ability to represent it are discussed in Supplementary Text S10. A positive, non-linear relationship between DOC and mean annual air temperature (MAAT), discussed in prior empirical studies, is also reproduced by the model (Fig. 7) and discussed in the Supplement Text S11.

4.6 DOC Reactivity Pools

Here we examine the reactivity of DOC leached from the soil and litter to different hydrological export pools. Surface runoff DOC export is dominated by refractory carbon (Fig. 9), with export rates largely following discharge rates as they drain the basin with an increasing delay when latitude increases. As the thaw period gets underway (April), the fraction of labile carbon in surface runoff DOC increases substantially from south to north, reflecting the hydrologic uptake of the previous year's un-decomposed high-reactivity organic matter.

Refractory C–dominated drainage DOC export (Fig. 9) is highest in June through October, with refractory export rate intensities per latitudinal band during this period consistent with the fraction of inundated area (Fig. S1b) over these bands during the year. The high refractory proportion of drainage flow is expected, as drainage leaches older, relict soil and litter matter. Because of its longer residence time within the soil column, labile DOC carried downward via soil infiltration will tend to be metabolised in situ before it can be exported to the hydrological network, further increasing the proportion of refractory carbon. By contrast floodplain DOC export (Fig. 9) is composed of more nuanced mix of both reactivity classes, reflecting its relatively greater dependence on the current year's 'fresh' biomass as source material (62% labile DOC versus 38% refractory DOC, year-averaged) for carbon leaching.

For both the river and stream pool, mean DOC concentrations are dominated by refractory carbon sources. When averaged over the year, the dominance of the refractory DOC carbon pool over its labile counterpart is also evident for all DOC inputs to the hydrological routing except for floodplain inputs, as well as within the 'flowing' stream and river pools themselves. This is shown in Table 2, where the year-averaged percentage of each carbon component of the total input or reservoir is subdivided between the 'North' and 'South' of the basin, these splits being arbitrarily imposed as the latitudinal mid-point of the basin itself (63N). This reinforces the generalised finding from our simulations that refractory carbon dominates runoff and drainage inflows to rivers (89% refractory, on average), while floodplains export mostly labile DOC to the basin (64%), these values being effectively independent of this latitudinal sub-division (Table 2). Nonetheless, there is a small consistent difference between North and South

392 in stream and river water DOC makeup, in that the labile portion decreases between
393 North and South ; this may be an attenuated reflection of the portion of labile DOC that is
394 decomposed to CO_2 within the water column during its transport northward, affecting
395 the bulk average proportions contained within the water in each 'hemisphere'.
396
397 **5 Discussion**
398
399 **5.1 Land-Ocean Aquatic Continuum (LOAC)**
400 **5.1.1 LOAC Fluxes**
401
402 Overall, our simulation results show that dissolved carbon entering the Lena river
403 system is significantly transformed during its transport to the ocean. Taking the average
404 throughput of carbon into the system over the last ten years of our simulation, our
405 results show that whereas 7 TgC yr^{-1} (after reinfiltration following flooding of 0.45 TgC
406 yr^{-1}; see Fig. 2 'Return' flux) of carbon enters the Lena from terrestrial sources as
407 dissolved carbon and CO_2, only 3.4 TgC yr^{-1} is discharged into the Laptev Sea and beyond
408 from the river mouth. The remainder (3.6TgC yr^{-1}) is metabolised in the water column
409 during transport and evaded to the atmosphere (bottom panel, Fig. 10). The terrestrial
410 DOC inflow estimate is comparable to that made by Kicklighter et al. (2013), who
411 estimated in a modelling study terrestrial dissolved carbon loading of the Lena is ~7.7
412 TgC yr^{-1}.
413
414 The relative quantities of carbon inflow, evasion and outflow in the river system that are
415 presented for the Lena in Fig. 10 can be compared to the same relative quantities –that
416 is, the ratios of evasion:in and out:in, where 'in' refers to dissolved terrestrial input, –
417 from the global study by Cole et al. (2007), who estimated these fluxes from empirical or
418 empirically-derived data at the global scale.   This is shown in the top panel of Fig. 10,
419 where we simplify the Cole et al. (2007) data to exclude global groundwater CO_2 flux
420 from the coast to the ocean (because our basin mask has a single coastal pixel whereas
421 coastal groundwater seepage is distributed along the entire continental boundary) and
422 the POC fraction of in-river transport and sedimentation (since ORCHIDEE MICT lacks a
423 POC erosion/sedimentation module) from their budget.
424
425 This gives global terrestrial dissolved carbon input of 1.45 PgC yr^{-1}, 0.7 PgC of which is
426 discharged to the ocean, and the other 0.75 PgC evaded to the atmosphere. Taking the
427 previously mentioned [evasion:in] and [out:in] ratios as a percentage, the outflow and
428 evasion fluxes for the Lena versus the global aggregate are remarkably similar, at 48.6
429 vs. 48.3% and 51.4 vs 51.7%, for the two respective flows. Thus our results agree with
430 the proposition that the riverine portion of the 'land-ocean aquatic continuum' (Regnier
431 et al., 2013) or 'boundless carbon cycle' (Battin et al., 2009) is indeed a substantial
432 reactor for matter transported along it. The drivers of changes in CO_2 and DOC export
433 from the soil over the simulation period (temperature and precipitation versus CO_2),
434 which we extract from our constant climate and CO_2 factorial simulations discussed in
435 the Simulation Setup, are similar, if somewhat dominated by temperature (Text S12).
436
437 **5.1.2 LOAC export flux considerations**
438
439 Despite our simulations' agreement with observations regarding the proportional fate of
440 terrestrial DOC inputs as evasion and marine export (Fig. 10), our results suggest

441 substantial and meaningful differences in the magnitude of those fluxes relative to NPP
442 in the Lena, compared to those estimated by other studies in temperate or tropical
443 biomes. Our simulations' cumulative DOC and CO_2 export from the terrestrial realm into
444 inland waters is equivalent to ~1.5 % of NPP.
445
446 This is considerably lower than Cole et al. (2007) and Regnier et al. (2013) who find
447 lateral transfer to approximate ~5% (1.9PgC yr^{-1}) of NPP at the global scale, while
448 Lauerwald et al. (2017) found similar rates for the Amazon. The cause of this
449 discrepancy with our results is beyond the scope of this study to definitively address,
450 given the lack of tracers for carbon source and age in our model. Nonetheless, our
451 analysis leads us to hypothesise the following.
452
453 Temperature limitation of soil microbial respiration at the end of the growing season
454 (approaching zero by October, SI Fig. S4d) makes this flux neglible from November
455 through May (SI Fig. S4d). In late spring, mobilisation of organic carbon is performed by
456 both microbial respiration and leaching of DOC via runoff and drainage water fluxes.
457 However, because the latter are controlled by the initial spring meltwater flux period,
458 which occurs before the growing season has had time to produce litter or new soil
459 carbon (May-June, Fig. 4b), aggregate yearly DOC transport reactivity is characterised by
460 the available plant matter from the previous year, which is overwhelmingly derived
461 from recalcitrant soil matter (Fig. 9) and is itself less available for leaching based on soil
462 carbon residence times.
463
464 This causes relatively low leaching rates and riverine DOC concentrations (e.g. Fig. 7), as
465 compared to the case of leaching from the same year's biological production.
466 Highlighting this point is floodplain domination by labile carbon sourced from that
467 year's production with a mean DOC concentration of 12.4 mgC L^{-1} (1998-2007 average),
468 with mean riverine DOC concentrations around half that value (6.9 mgC L^{-1}).
469 Nonetheless the May-June meltwater pulse period dominates aggregate DOC discharge.
470 As this pulse rapidly subsides by late July, so does the leaching and transport of organic
471 matter. Warmer temperatures come in conjunction with increased primary production
472 and the temperature driven soil heterotrophic degradation of contemporary and older
473 matter (via active layer deepening). These all indicate that transported dissolved matter
474 in rivers, at least at peak outflow, is dominated by sources originating in the previous
475 year's primary production, that was literally 'frozen out' of more complete
476 decomposition by soil heterotrophs.
477
478 Further, we infer from the fact that all of our simulation grid cells fall within areas of low
479 (<-2°C) MAAT, far below the threshold MAAT (>3°C) proposed by Laudon et al. (2012)
480 for soil respiration-dominated carbon cycling systems (Fig. 7), that the Lena is
481 hydrologically-limited with respect to DOC concentration and its lateral flux. Indeed, the
482 seasonal discharge trend of the Lena –massive snowmelt-driven hydrological and
483 absolute DOC flux, coupled with relatively low DOC concentrations at the river mouth
484 (Fig. 4b, simulation data of Fig. 7), are in line with the Laudon et al. (2012) typology.
485
486 We therefore suggest that relatively low lateral transport relative to primary production
487 rates (e.g. as a percentage of net primary production, (%NPP)) in our simulations
488 compared to the lateral transport : NPP percentages reported from the literature in
489 other biomes is driven by meltwater (vs. precipitation) dominated DOC mobilisation,

490 which occurs during a largely pre-litter deposition period of the growing season. DOC is
491 then less readily mobilised by being sourced from recalcitrant matter, leading to low
492 leaching concentrations relative to those from labile material. As discharge rates
493 decline, the growing season reaches its peak, leaving carbon mobilisation of fresh
494 organic matter to be overwhelmingly driven by in situ heterotrophic respiration.
495
496 While we have shown that bulk DOC fluxes scale linearly to bulk discharge flows (Fig.
497 3d), DOC concentrations (mgC L^{-1}) hold a more complex and weaker positive
498 relationship with discharge rates, with correlation coefficients (R^2) of 0.05 and 0.25 for
499 river and stream DOC concentrations, respectively (Fig. 13). This implies that while
500 increasing discharge reflects increasing runoff and an increasing vector for DOC
501 leaching, particularly in smaller tributary streams, by the time this higher input of
502 carbon reaches the river main stem there is a confounding effect of dilution by increased
503 water fluxes which reduces DOC concentrations, explaining the difference between
504 stream and river discharge vs. DOC concentration regressions in the Figure. Thus, and
505 as a broad generalisation, with increasing discharge rates we can also expect somewhat
506 higher concentrations of terrestrial DOC input to streams and rivers. Over the
507 floodplains, DOC concentrations hold no linear relationship with discharge rates
508 (R^2=0.003 , SI Fig. S11), largely reflecting the fact that DOC leaching is here limited by
509 terrestrial primary production rates more than by hydrology. To the extent that
510 floodplains fundamentally require flooding and hence do depend on floodwater inputs
511 at a primary level, we hypothesise that DOC leaching rates are not limited by that water
512 input, at least over the simulated Lena basin.
513
514 As discussed above simulated DOC and CO$_2$ export as a percentage of simulated NPP
515 over the Lena basin was 1.5% over 1998-2007. However, this proportion appears to be
516 highly dynamic at the decadal timescale. As shown in Fig. S12, all lateral flux
517 components in our simulations increased their relative throughput at a rate double to
518 triple that of NPP or respiration fluxes over the 20th century, also doing so at a rate
519 substantially higher than the rate increase in discharge. In addition, differentials of
520 these lateral flux rates with the rates of their drivers (discharge, primary production)
521 have on average increased over the century (Fig. S12). This suggests that there are
522 potential additive effects of the production and discharge drivers of lateral fluxes that
523 could lead to non-linear responses to changes in these drivers as the Arctic environment
524 transforms, as suggested by the Laudon et al. (2012) data plotted in Fig. 4. Acceleration
525 of the hydrological cycle compounded by temperature and CO$_2$ -driven increases in
526 primary production could therefore increase the amount of matter available for
527 leaching, increase the carbon concentration of leachate, and increase the aggregate
528 generation of runoff to be used as a DOC transport vector. Given that these causal
529 dynamics apply generally to permafrost regions, both low lateral flux as %NPP and the
530 hypothesised response of those fluxes to future warming may be a feature particular to
531 most high latitude river basins.
532
533 **6. Conclusion**
534
535 This study has shown that the new DOC-representing high latitude model version of
536 ORCHIDEE, ORCHIDEE MICT-LEAK, is able to reproduce with reasonable accuracy
537 modern concentrations, rates and absolute fluxes of carbon in dissolved form, as well as
538 the relative seasonality of these quantities through the year. When combined with a

reasonable reproduction of real-world stream, river and floodplain dynamics, we demonstrate that this model is a potentially powerful new tool for diagnosing and reproducing past, present and potentially future states of the Arctic carbon cycle. Our simulations show that of the 34 TgC yr^{-1} remaining after GPP is respired autotrophically and heterotrophically in the Lena basin, over one-fifth of this captured carbon is removed into the aquatic system. Of this, over half is released to the atmosphere from the river surface during its period of transport to the ocean, in agreement with previous empirically-derived global-scale studies. Both this transport and its transformation are therefore non-trivial components of the carbon system at these latitudes that we have shown are sensitive to changes in temperature, precipitation and atmospheric CO_2 concentration. Our results, in combination with empirical data, further suggest that changes to these drivers –in particular climate –may provoke non-linear responses in the transport and transformation of carbon across the terrestrial-aquatic system's interface as change progresses in an Arctic environment increasingly characterised by amplified warming.

Code and data availability

The source code for ORCHIDEE MICT-LEAK revision 5459 is available via http://forge.ipsl.jussieu.fr/orchidee/wiki/GroupActivities/CodeAvalaibilityPublication/ORCHIDEE_gmd-2018-MICT-LEAK_r5459

Primary data and scripts used in the analysis and other supplementary information that may be useful in reproducing the author's work can be obtained by contacting the corresponding author.

This software is governed by the CeCILL license under French law and abiding by the rules of distribution of free software. You can use, modify and/or redistribute the software under the terms of the CeCILL license as circulated by CEA, CNRS and INRIA at the following URL: http://www.cecill.info.

Authors' contribution

SB coded this model version, conducted the simulations and wrote the main body of the paper. RL gave consistent input to the coding process and made numerous code improvements and bug fixes. BG advised on the inclusion of priming processes in the model and advised on the study design and model configuration; DZ gave input on the modelled soil carbon processes and model configuration. PR contributed to the interpretation of results and made substantial contributions to the manuscript text. MG, AT and AD contributed to improvements in hydrological representation and floodplain forcing data. PC oversaw all developments leading to the publication of this study. All authors contributed to suggestions regarding the final content of the study.

Competing interests

The authors declare no competing financial interests.

592
593

References:

595
596 Battin, T. J., Luyssaert, S., Kaplan, L. A., Aufdenkampe, A. K., Richter, A. and Tranvik, L. J.:
597 The boundless carbon cycle, Nat. Geosci., doi:10.1038/ngeo618, 2009.
598 Cauwet, G. and Sidorov, I.: The biogeochemistry of Lena River: Organic carbon and
599 nutrients distribution, in Marine Chemistry, pp. 211–227., 1996.
600 Cole, J. J., Prairie, Y. T., Caraco, N. F., McDowell, W. H., Tranvik, L. J., Striegl, R. G., Duarte,
601 C. M., Kortelainen, P., Downing, J. A., Middelburg, J. J. and Melack, J.: Plumbing the global
602 carbon cycle: Integrating inland waters into the terrestrial carbon budget, Ecosystems,
603 doi:10.1007/s10021-006-9013-8, 2007.
604 DeLuca, T. H. and Boisvenue, C.: Boreal forest soil carbon: Distribution, function and
605 modelling, Forestry, 161–184, doi:10.1093/forestry/cps003, 2012.
606 Dolman, A. J., Shvidenko, A., Schepaschenko, D., Ciais, P., Tchebakova, N., Chen, T., Van
607 Der Molen, M. K., Belelli Marchesini, L., Maximov, T. C., Maksyutov, S. and Schulze, E. D.:
608 An estimate of the terrestrial carbon budget of Russia using inventory-based, eddy
609 covariance and inversion methods, Biogeosciences, doi:10.5194/bg-9-5323-2012, 2012.
610 Guimberteau, M., Zhu, D., Maignan, F., Huang, Y., Yue, C., Dantec-N d lec, S., Ottl, C., Jornet-
611 Puig, A., Bastos, A., Laurent, P., Goll, D., Bowring, S., Chang, J., Guenet, B., Tifafi, M., Peng,
612 S., Krinner, G., Ducharne, A. s., Wang, F., Wang, T., Wang, X., Wang, Y., Yin, Z., Lauerwald,
613 R., Joetzjer, E., Qiu, C., Kim, H. and Ciais, P.: ORCHIDEE-MICT (v8.4.1), a land surface
614 model for the high latitudes: model description and validation, Geosci. Model Dev.,
615 11(1), 121–163, doi:10.5194/gmd-11-121-2018, 2018.
616 Holmes, R. M., McClelland, J. W., Peterson, B. J., Tank, S. E., Bulygina, E., Eglinton, T. I.,
617 Gordeev, V. V., Gurtovaya, T. Y., Raymond, P. A., Repeta, D. J., Staples, R., Striegl, R. G.,
618 Zhulidov, A. V. and Zimov, S. A.: Seasonal and Annual Fluxes of Nutrients and Organic
619 Matter from Large Rivers to the Arctic Ocean and Surrounding Seas, Estuaries and
620 Coasts, 35(2), 369–382, doi:10.1007/s12237-011-9386-6, 2012.
621 Jasechko, S., Kirchner, J. W., Welker, J. M. and McDonnell, J. J.: Substantial proportion of
622 global streamflow less than three months old, Nat. Geosci., 9(2), 126,
623 doi:10.1038/ngeo2636, 2016.
624 Kalnay, E., Kanamitsu, M., Kistler, R., Collins, W., Deaven, D., Gandin, L., Iredell, M., Saha,
625 S., White, G., Woollen, J., Zhu, Y., Chelliah, M., Ebisuzaki, W., Higgins, W., Janowiak, J., Mo,
626 K. C., Ropelewski, C., Wang, J., Leetmaa, A., Reynolds, R., Jenne, R. and Joseph, D.: The
627 NCEP/NCAR 40-year reanalysis project, Bull. Am. Meteorol. Soc., doi:10.1175/1520-
628 0477(1996)077<0437:TNYRP>2.0.CO;2, 1996.
629 Kicklighter, D. W., Hayes, D. J., Mcclelland, J. W., Peterson, B. J., Mcguire, A. D. and Melillo,
630 J. M.: Insights and issues with simulating terrestrial DOC loading of Arctic river
631 networks, Ecol. Appl., 23(8), 1817–1836, doi:10.1890/11-1050.1, 2013.
632 Kutscher, L., Mörth, C. M., Porcelli, D., Hirst, C., Maximov, T. C., Petrov, R. E. and
633 Andersson, P. S.: Spatial variation in concentration and sources of organic carbon in the
634 Lena River, Siberia, J. Geophys. Res. Biogeosciences, 122(8), 1999–2016,
635 doi:10.1002/2017JG003858, 2017.
636 Lara, R. J., Rachold, V., Kattner, G., Hubberten, H. W., Guggenberger, G., Skoog, A. and

637 Thomas, D. N.: Dissolved organic matter and nutrients in the Lena River, Siberian Arctic:
638 Characteristics and distribution, Mar. Chem., doi:10.1016/S0304-4203(97)00076-5,
639 1998.
640 Lauerwald, R., Regnier, P., Camino-Serrano, M., Guenet, B., Guimberteau, M., Ducharne,
641 A., Polcher, J. and Ciais, P.: ORCHILEAK (revision 3875): A new model branch to simulate
642 carbon transfers along the terrestrial-aquatic continuum of the Amazon basin, Geosci.
643 Model Dev., 10, 3821–3859, doi:10.5194/gmd-10-3821-2017, 2017.
644 McGuire, K. J., McDonnell, J. J., Weiler, M., Kendall, C., McGlynn, B. L., Welker, J. M. and
645 Seibert, J.: The role of topography on catchment-scale water residence time, Water
646 Resour. Res., doi:10.1029/2004WR003657, 2005.
647 New, M., Hulme, M. and Jones, P.: Representing twentieth-century space-time climate
648 variability. Part I: Development of a 1961-90 mean monthly terrestrial climatology, J.
649 Clim., 1999.
650 Raymond, P. A., McClelland, J. W., Holmes, R. M., Zhulidov, A. V., Mull, K., Peterson, B. J.,
651 Striegl, R. G., Aiken, G. R. and Gurtovaya, T. Y.: Flux and age of dissolved organic carbon
652 exported to the Arctic Ocean: A carbon isotopic study of the five largest arctic rivers,
653 Global Biogeochem. Cycles, 21(4), doi:10.1029/2007GB002934, 2007.
654 Regnier, P., Friedlingstein, P., Ciais, P., Mackenzie, F. T., Gruber, N., Janssens, I. A.,
655 Laruelle, G. G., Lauerwald, R., Luyssaert, S., Andersson, A. J., Arndt, S., Arnosti, C., Borges,
656 A. V., Dale, A. W., Gallego-Sala, A., Goddéris, Y., Goossens, N., Hartmann, J., Heinze, C.,
657 Ilyina, T., Joos, F., Larowe, D. E., Leifeld, J., Meysman, F. J. R., Munhoven, G., Raymond, P.
658 A., Spahni, R., Suntharalingam, P. and Thullner, M.: Anthropogenic perturbation of the
659 carbon fluxes from land to ocean, Nat. Geosci., doi:10.1038/ngeo1830, 2013.
660 Semiletov, I. P., Pipko, I. I., Shakhova, N. E., Dudarev, O. V., Pugach, S. P., Charkin, A. N.,
661 Mcroy, C. P., Kosmach, D. and Gustafsson, Ö.: Carbon transport by the Lena River from its
662 headwaters to the Arctic Ocean, with emphasis on fluvial input of terrestrial particulate
663 organic carbon vs. carbon transport by coastal erosion, Biogeosciences, doi:10.5194/bg-
664 8-2407-2011, 2011.
665 Tootchi, A., Jost, A. and Ducharne, A.: Multi-source global wetland maps combining
666 surface water imagery and groundwater constraints, Earth Syst. Sci. Data, 11, 189–220,
667 doi:10.5194/essd-11-189-2019, 2019.
668 Ye, B., Yang, D., Zhang, Z. and Kane, D. L.: Variation of hydrological regime with
669 permafrost coverage over Lena Basin in Siberia, J. Geophys. Res. Atmos., 114, D7,
670 doi:10.1029/2008JD010537, 2009.
671
672
673
674
675

676 **Tables and Figures:**
677
678 **Table 1:** Summary describing of the factorial simulations undertaken to examine the
679 relative drivers of lateral fluxes in our model.
680

Simulation Name	Abbreviation	Historical Input Data	Input* Held Constant
Control	CTRL	Climate, CO2, Vegetation	None
Constant Climate	CLIM	CO2, Vegetation	Climate
Constant CO2	CO2	Climate, Vegetation	CO2 (Pre-industrial)

*Historically-variable input

Table 2: Summary of the average carbon reactivity types comprising the hydrological inputs to rivers and streams (runoff, drainage and floodplain inputs), and within the rivers and streams themselves, subdivided between the 'North' and 'South' of the Lena basin (greater or less than 63N, respectively).

Hydrological Source	Model Carbon Reactivity Pool	North	South
Runoff Input	Refractory	81%	83%
	Labile	19%	17%
Drainage Input	Refractory	96%	94%
	Labile	4%	6%
Flood Input	Refractory	36%	37%
	Labile	64%	63%
Streams	Refractory	91%	89%
	Labile	9%	11%
Rivers	Refractory	92%	90%
	Labile	8%	10%
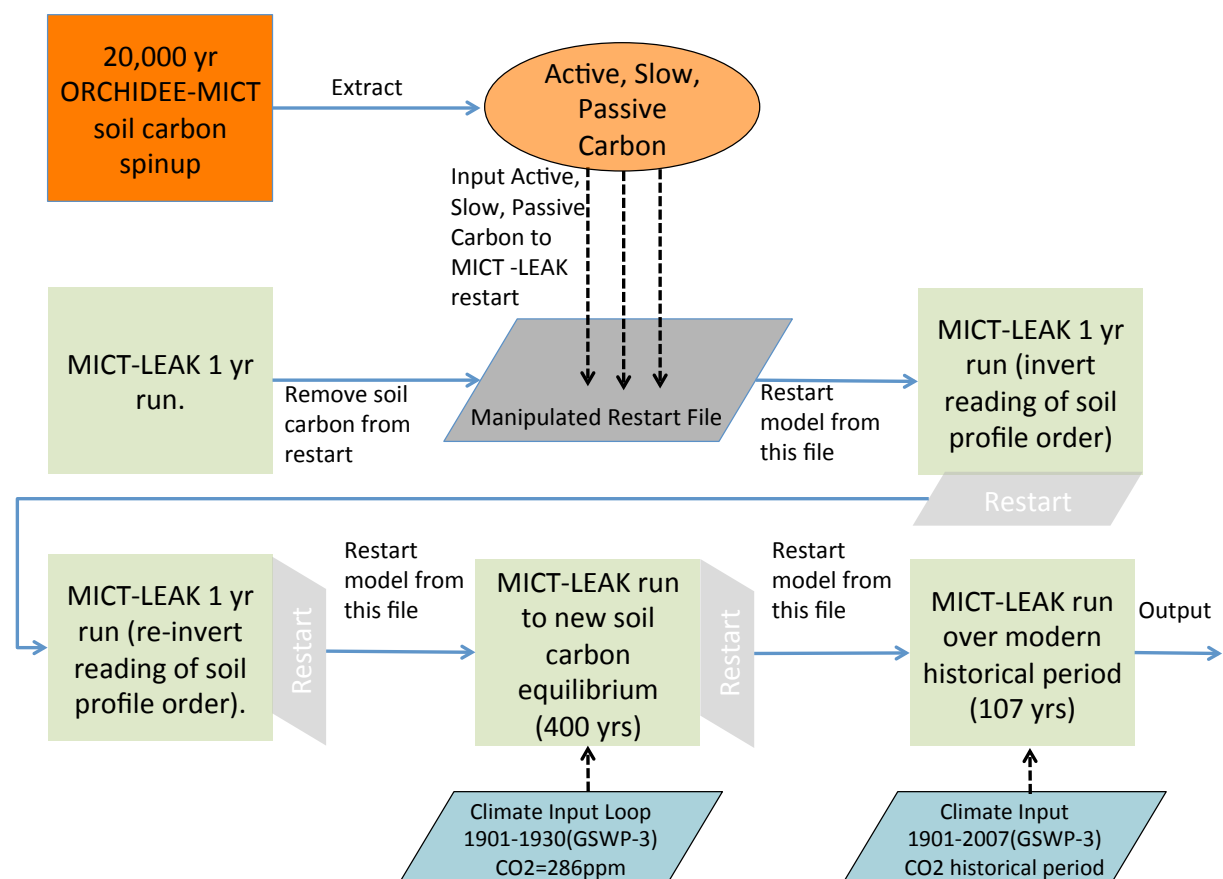
Figure 1: Flow diagram illustrating the step-wise stages required to set up the model, up to and including the historical period. The two stages that refer to the inverted reading of restart soil profile order point to the fact that the restart inputs from ORCHIDEE-MICT are read by our model in inverse order, so that one year must be run in

694 which an activated flag reads it properly, before the reading of soil profile restarts is re-
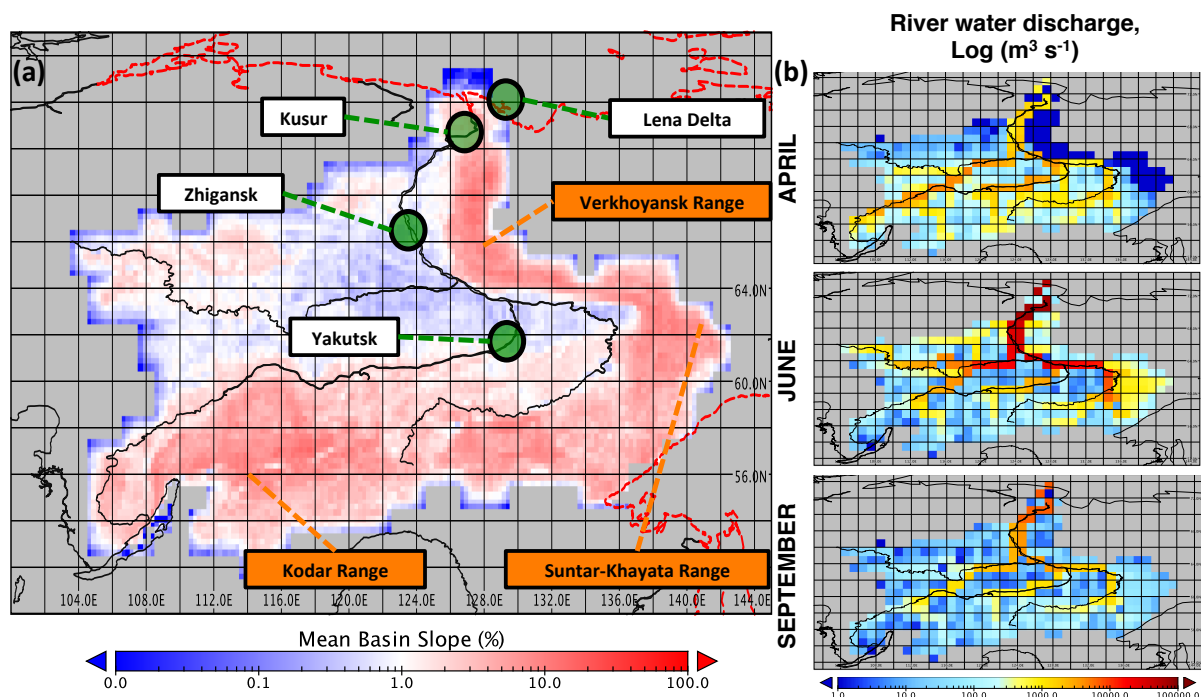695 inverted for all subsequent years.
696
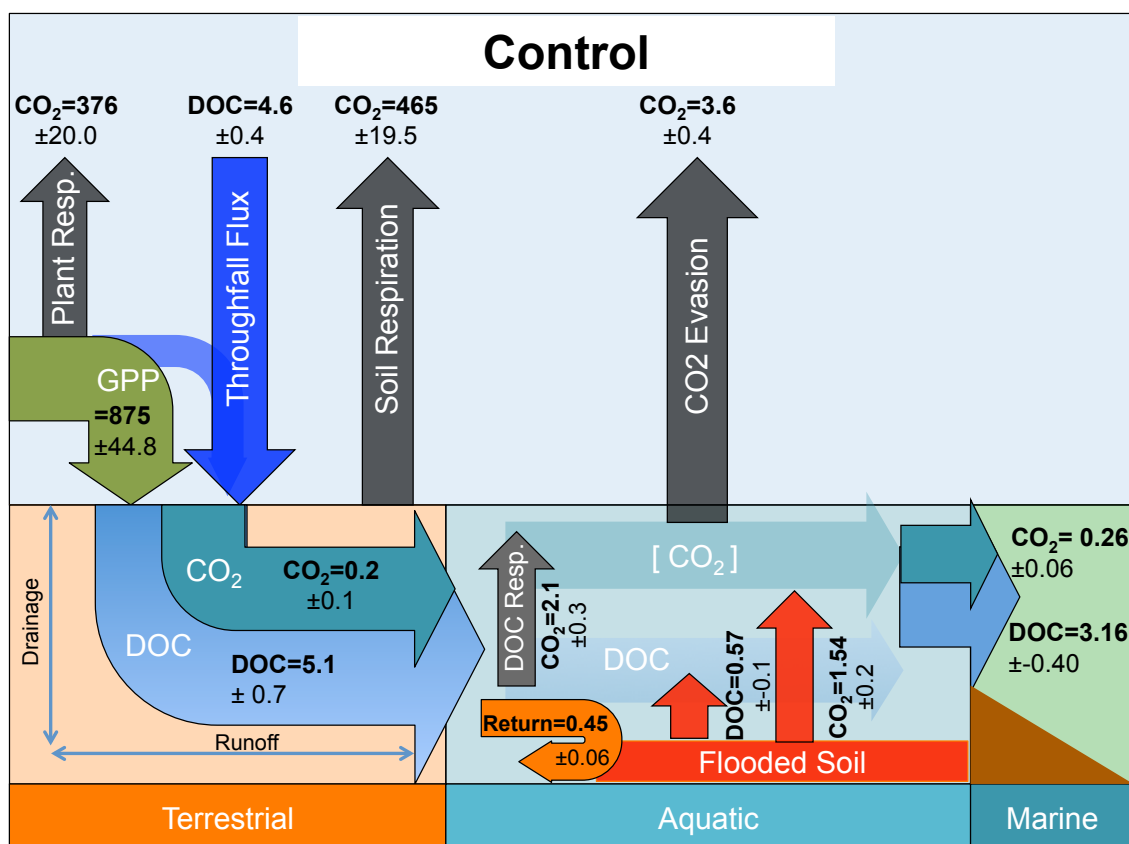
697
698 **Figure 2:** Schematic diagrams detailing the major yearly carbon flux outputs (TgC yr^{-1})
699 from the Control simulation averaged over the period 1998-2007 as they are
700 transformed and transported across the land-aquatic continuum.
701

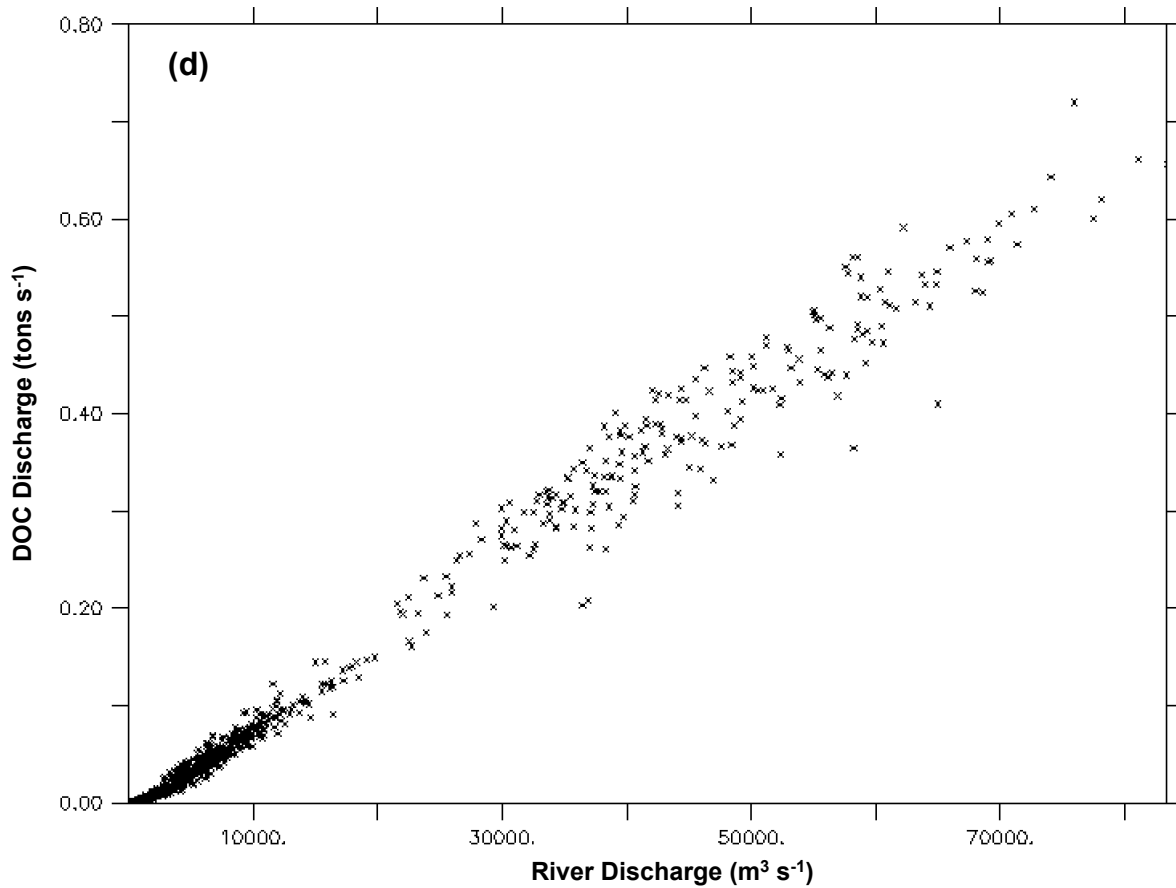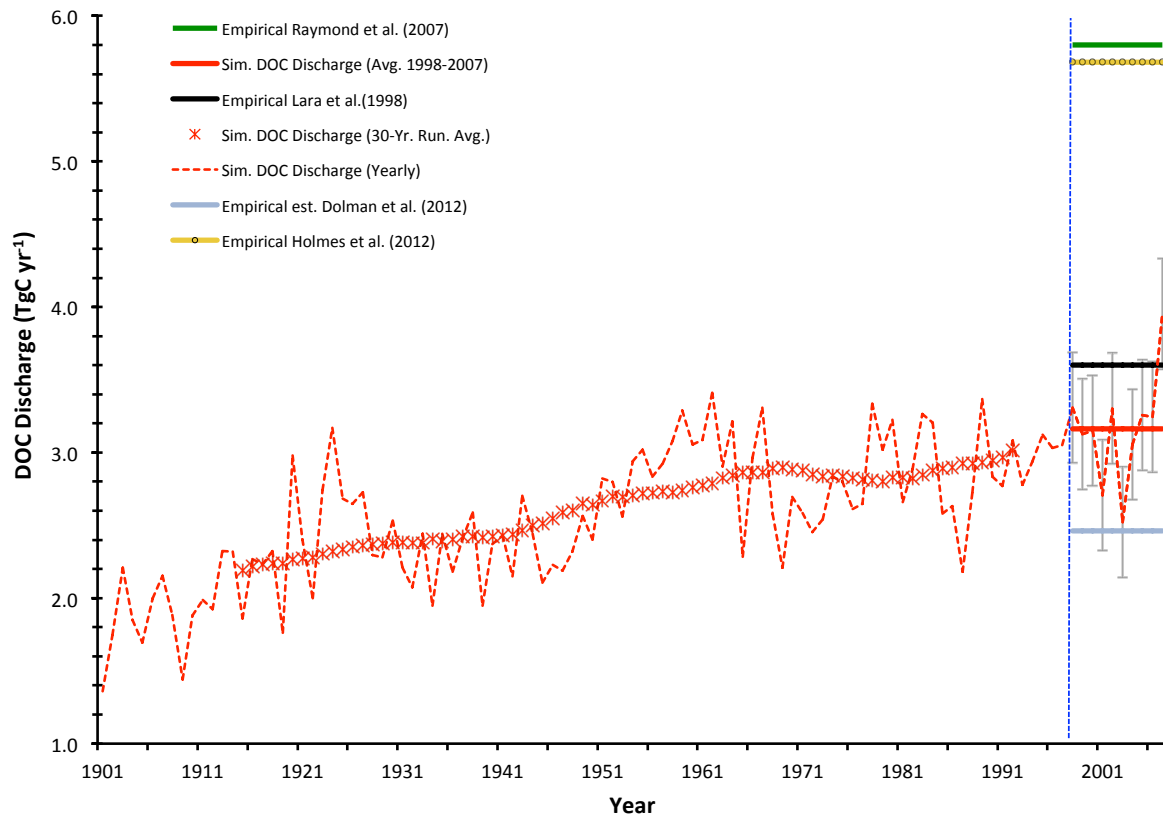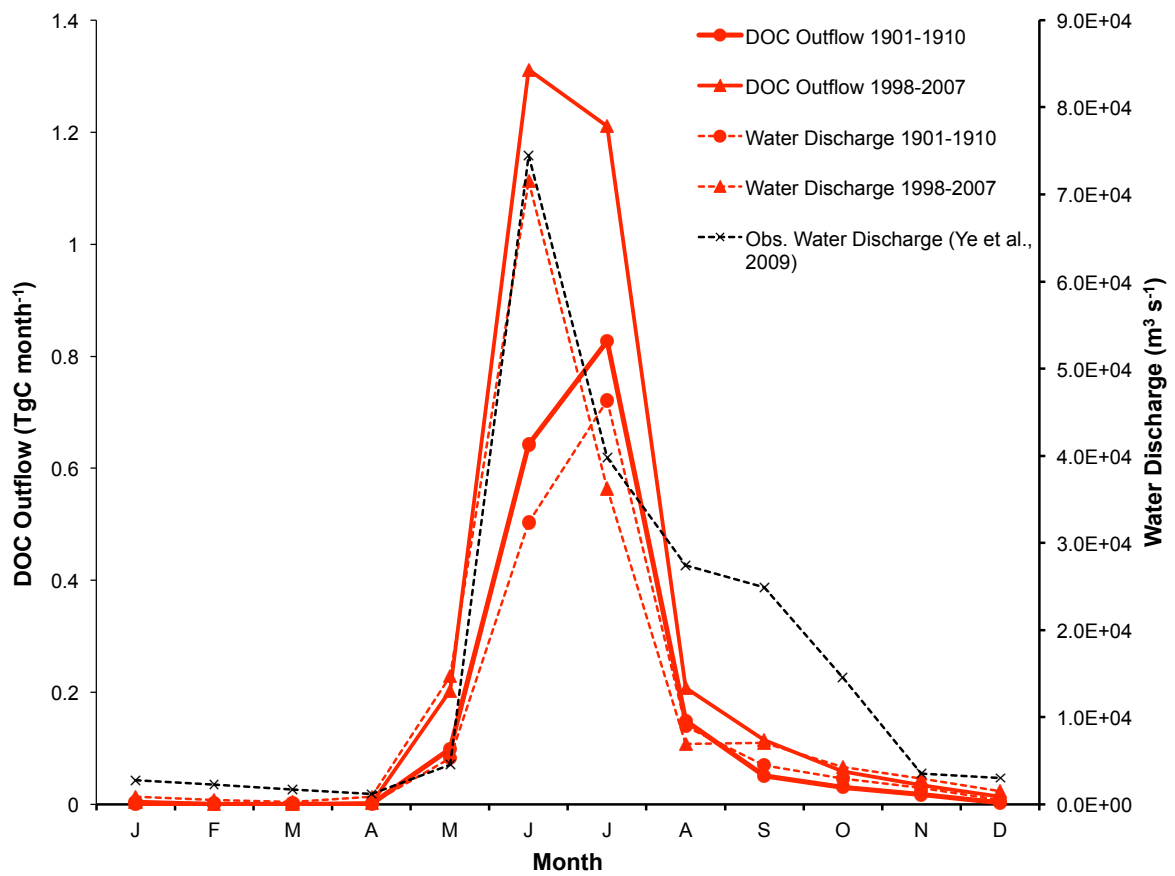**(a)** Kusur · Lena Delta · Zhigansk · Verkhoyansk Range · Yakutsk · Kodar Range · Suntar-Khayata Range

Mean Basin Slope (%)

0.0   0.1   1.0   10.0   100.0

(b) River water discharge, Log (m³ s⁻¹)

APRIL · JUNE · SEPTEMBER

1.0   10.0   100.0   1000.0   10000.0   100000.0

702
703
704

(c)

- Difference (Sim. - Obs.) River Discharge
- % Diff. (Sim. - Obs.) River Discharge

River Discharge Differential (m³ s⁻¹)

River Discharge Differential (%)

J F M A M J J A S O N D

705
706

707
708 **Figure 3**: Map of the Lena **(a)** with the scale bar showing the mean grid cell topographic
709 slope from the simulation, and the black line the satellite-derived overlay of the river
710 main stem and sub-basins. Mountain ranges of the Lena basin are shown in orange.
711 Green circles denote the outflow gridcell (Kusur) from which our simulation outflow
712 data are derived, as well as the Zhigansk site, from which out evaluation against data
713 from Raymond et al. (2007) are assessed. The regional capital (Yakutsk) is also included
714 for geographic reference. Coastal outline and inland water bodies are shown as dashed
715 red and solid black lines, respectively. **(b)** Maps of river water discharge ($\log(m^3\,s^{-1})$) in
716 April, June and September, averaged over 1998-2007. **(c)** The mean monthly river
717 discharge differential between observed discharge for the Lena (Ye et al., 2009) and
718 simulated discharge averaged over 1998-2007, in absolute ($m^3\ s^{-1}$) and percentage
719 terms. **(d)** Regression of simulated monthly DOC discharge versus simulated river
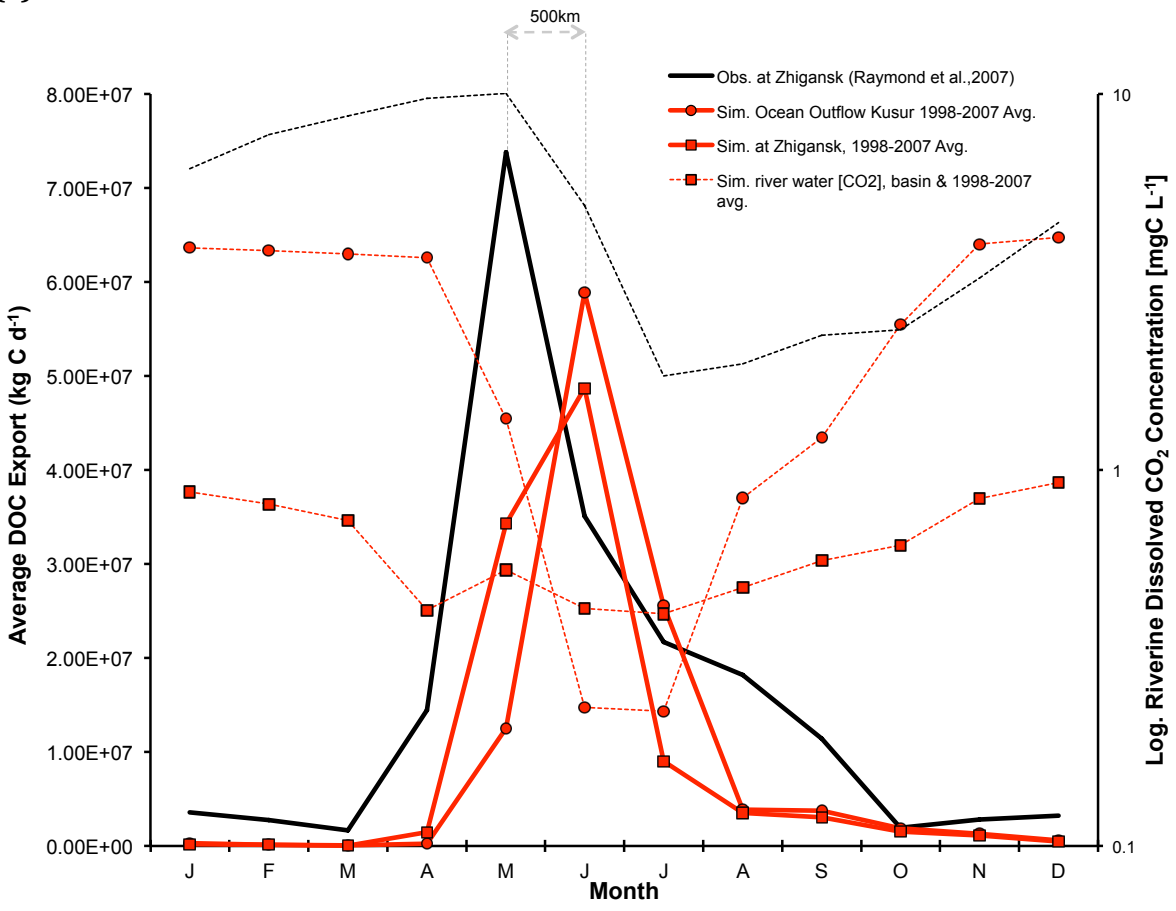720 discharge at the river mouth (Kusur) over the entire simulation period (1901-2007).
721
722 **(a)**

723
724 **(b)**
725

726

727 **(c)**

Figure with x-axis "Month" (J F M A M J J A S O N D), left y-axis "Average DOC Export (kg C d⁻¹)" ranging from 0.00E+00 to 8.00E+07, and right y-axis "Log. Riverine Dissolved CO₂ Concentration [mgC L⁻¹]" ranging from 0.1 to 10. Legend:
- Obs. at Zhigansk (Raymond et al.,2007)
- Sim. Ocean Outflow Kusur 1998-2007 Avg.
- Sim. at Zhigansk, 1998-2007 Avg.
- Sim. river water [CO2], basin & 1998-2007 avg.

728
729
730 **Figure 4: (a)** Yearly DOC discharged from the Lena river into the Laptev sea is shown
731 here in tC yr⁻¹, over the entire simulation period (dashed red line), with the smoothed,
732 30-year running mean shown in asterisk.   Observation based estimates for DOC
733 discharge from Lara et al. (1998), Raymond et al. (2007), Dolman et al. (2012) and
734 Holmes et al. (2012) are shown by the horizontal black, green triangle, blue diamond
735 and yellow circle line colours and symbols, respectively, and are to be compared against
736 the simulated mean over the last decade of simulation (1998-2007, horizontal red line),
737 with error bars added in grey displaying the standard deviation of simulated values over
738 that period. **(b)** Average monthly DOC discharge (solid red, tC month⁻¹) and water
739 discharge (dashed red, m³ s⁻¹) to the Laptev Sea over the period averaged for 1901-1910
740 (circles) and 1997-2007 (squares) are compared, with modern maxima closely tracking
741 observed values.   Observed water discharge over 1936-2000 from R-ArcticNet v.4
742 (Lammers et al., 2001) and published in Ye et al. (2009) are shown by the dashed black
743 line. **(c)** Observed (black) and simulated (red) seasonal DOC fluxes (solid lines) and CO_2
744 discharge concentrations (dashed lines). Observed DOC discharge as published in
745 Raymond et al. (2007) from 2004-2005 observations at Zhigansk, a site ~500km
746 upstream of the Lena delta. This is plotted against simulated discharge for: (i) the Lena
747 delta at Kusur (red circles) and (ii) the approximate grid pixel corresponding to the
748 Zhigansk site (red squares) averaged over 1998-2008. Observed CO_2 discharge from a
749 downstream site (Cauwet & Sidorov, 1996; dashed black), and simulated from the
750 outflow site (dashed circle) and the basin average (dashed square) are shown on the
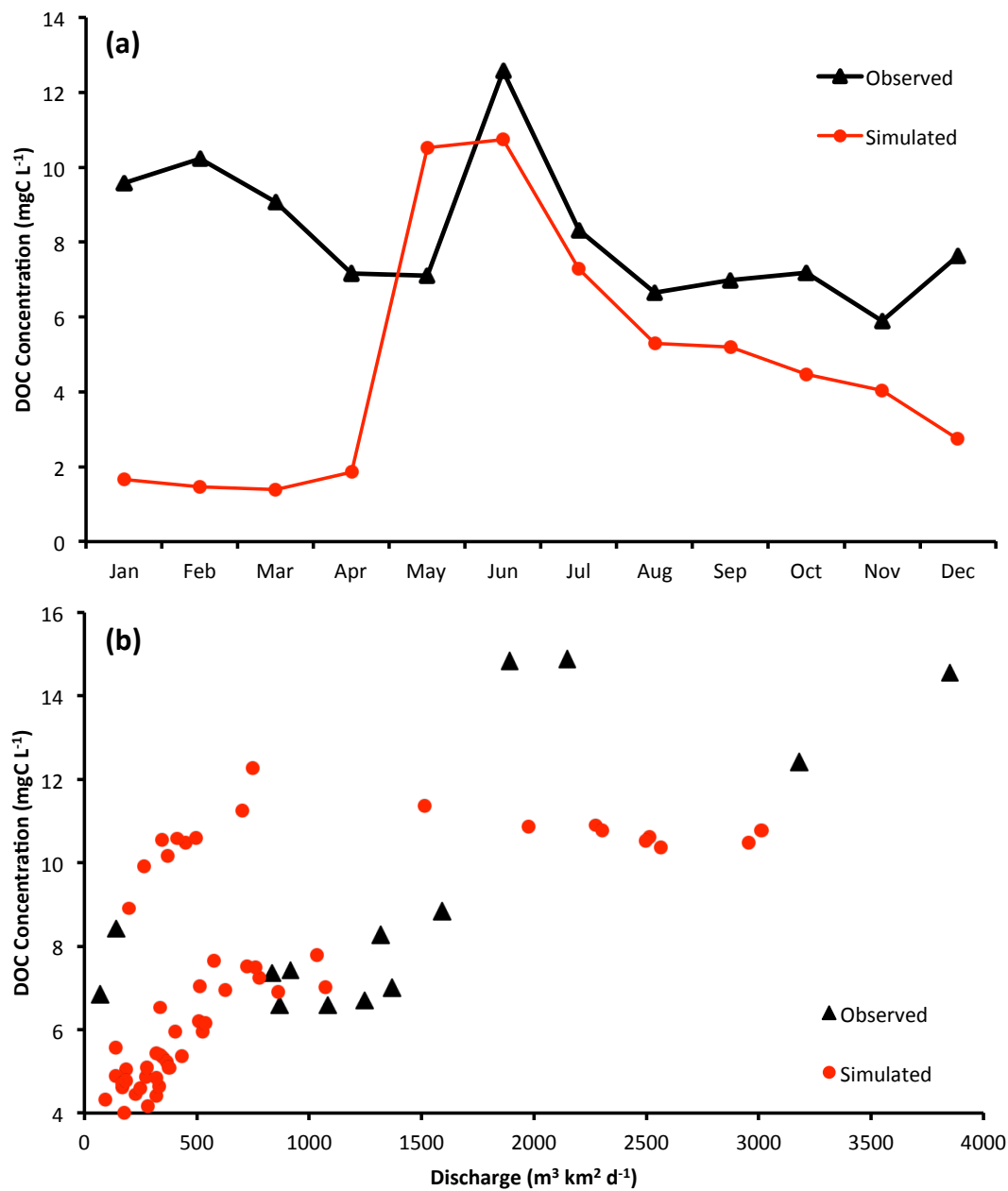751 log-scale right-hand axis for 1998-2008.

752
753 **Figure 5: (a)** Simulated and observed (Arctic-GRO/Holmes et al., 2012) DOC
754 concentration seasonality for the Lena basin over the period 1999-2007. **(b)** Plots of
755 DOC concentration versus river discharge as in observations (Raymond et al., 2007) and
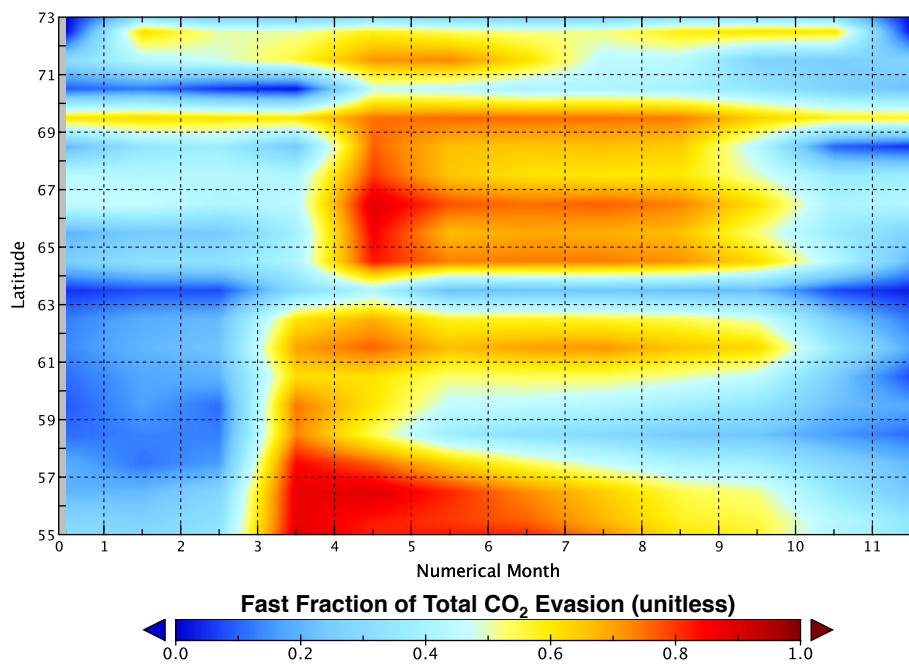756 simulations, where simulations data points are monthly averages taken over the period
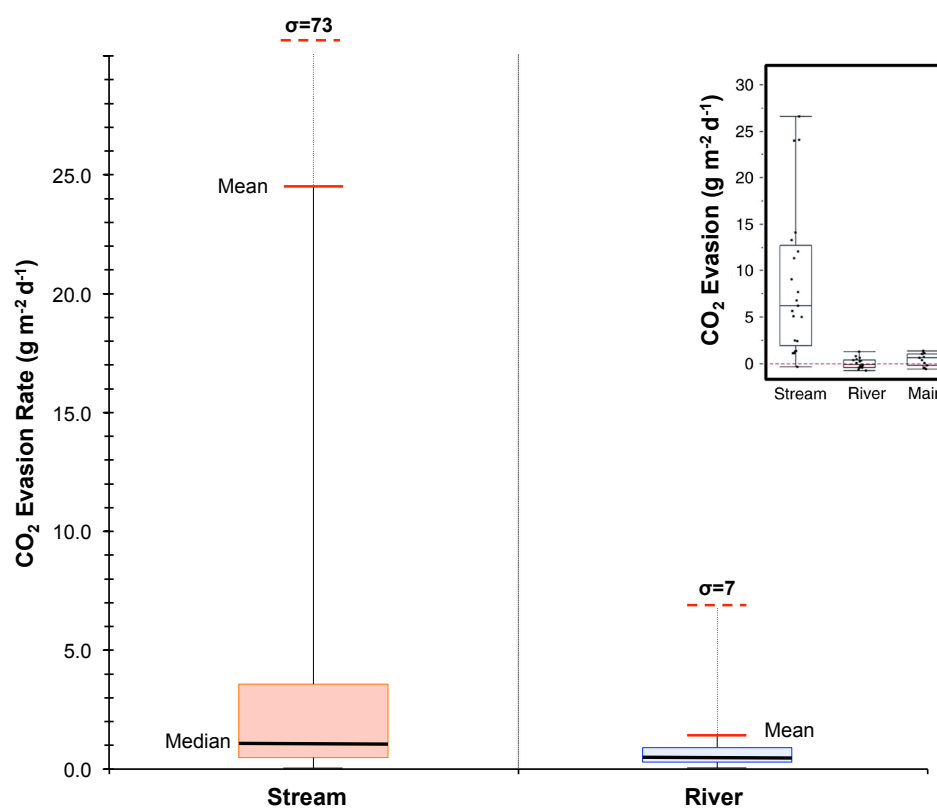757 1999-2007
758
759
760 **(a)**

761
762 **(b)**
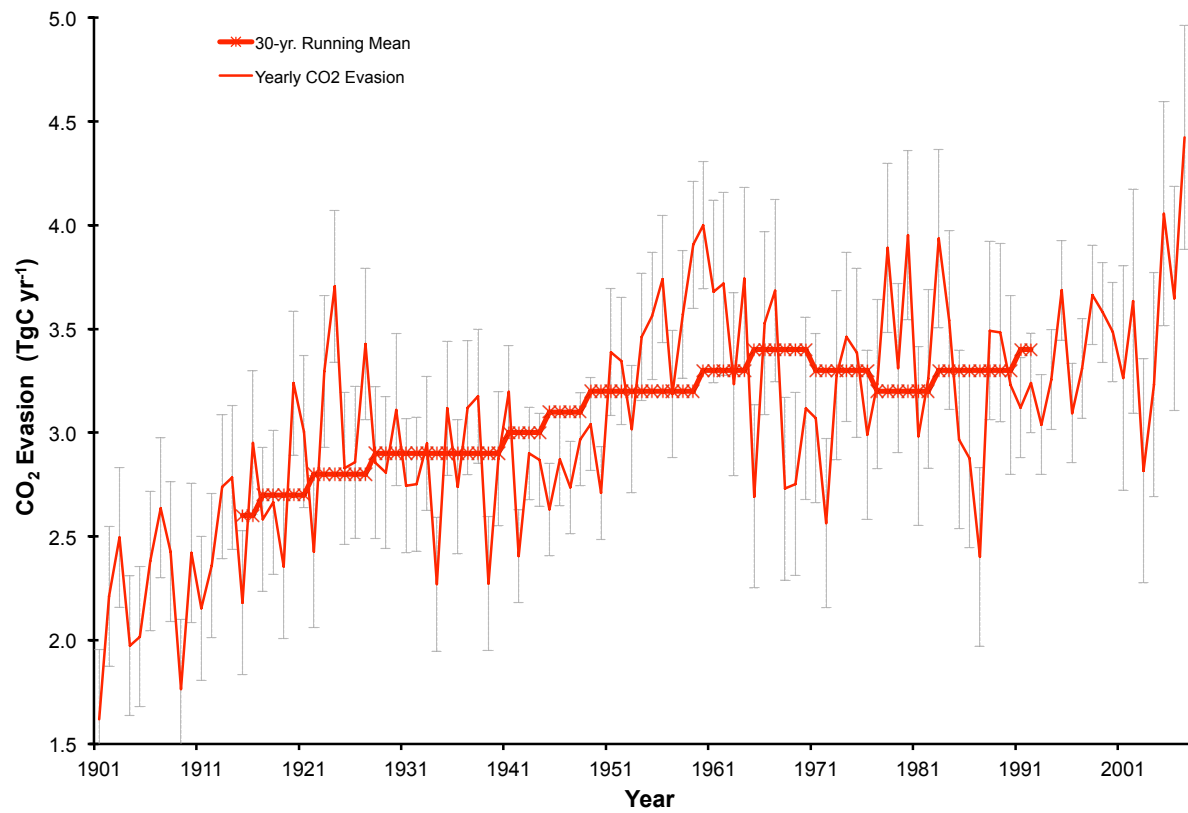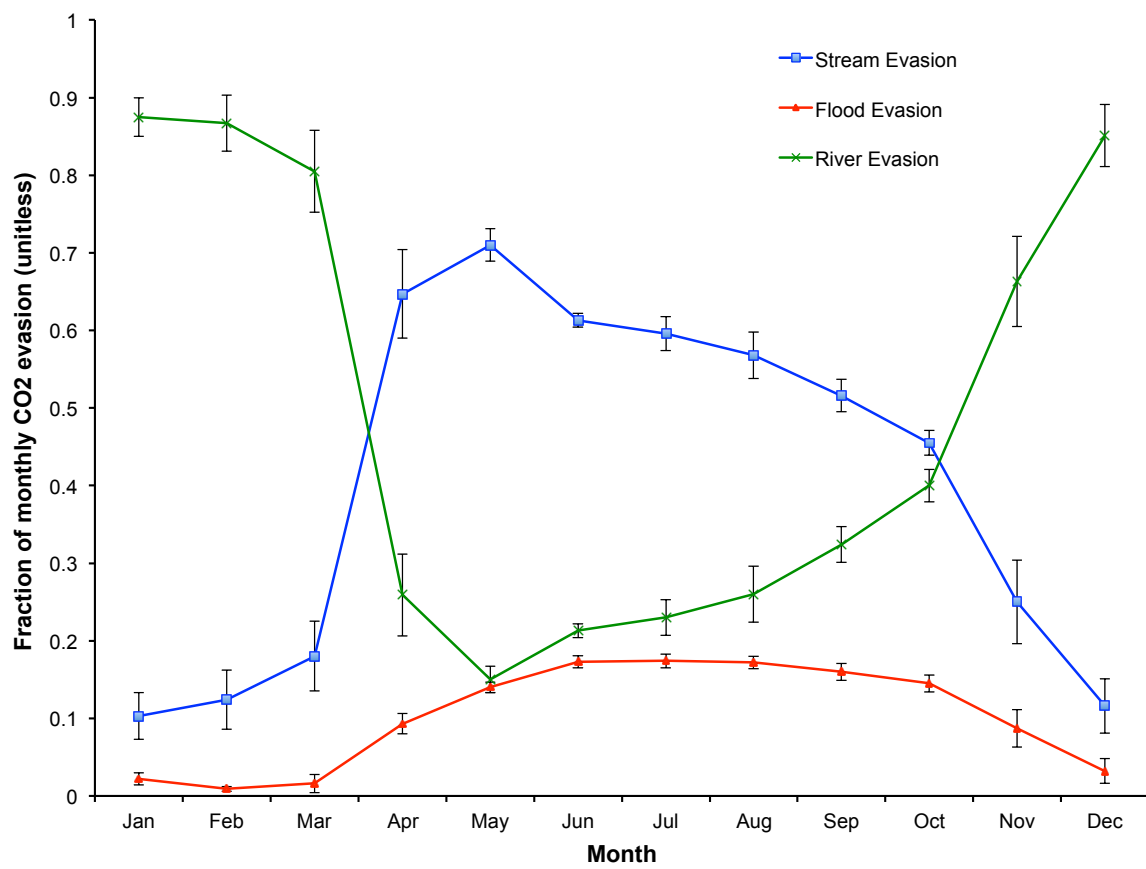
763
764 **(c)**

(d)

Figure 6: CO_2 evasion from stream, river, flood reservoirs. **(a)** Timeseries of total yearly CO_2 evasion (tC yr^{-1}) summed over the three hydrological pools (red line) with

774 the 30-year running mean of the same variable overlain in thick red (asterisk). Error
775 bars give the standard deviation of each decade (e.g. 1901-1910) for each data point in
776 that decade. **(b)** The fraction of total CO_2 evasion emitted from each of the hydrological
777 pools for the average of each month over the period 1998-2007 is shown for river, flood
778 and stream pools (blue, green and red lines, respectively), with error bars depicting the
779 standard deviation of data values for each month displayed. **(c)** Hovmöller diagram
780 showing the monthly evolution of the stream pool fraction (range 0-1) per month and
781 per latitudinal band, averaged over the period 1998-2007. **(d)** Boxplot for approximate
782 (see text) simulated CO_2 evasion (gC m^{-2} d^{-1}) from the streamwater reservoir and river
783 water reservoir averaged over 1998-2007. Coloured boxes denote the first and third
784 quartiles of the data range, internal black bars the median. Whiskers give the mean
785 (solid red bar) and standard deviation (dashed red bar) of the respective data.
786 Empirical data on these quantities using the same scale for rivers, streams and
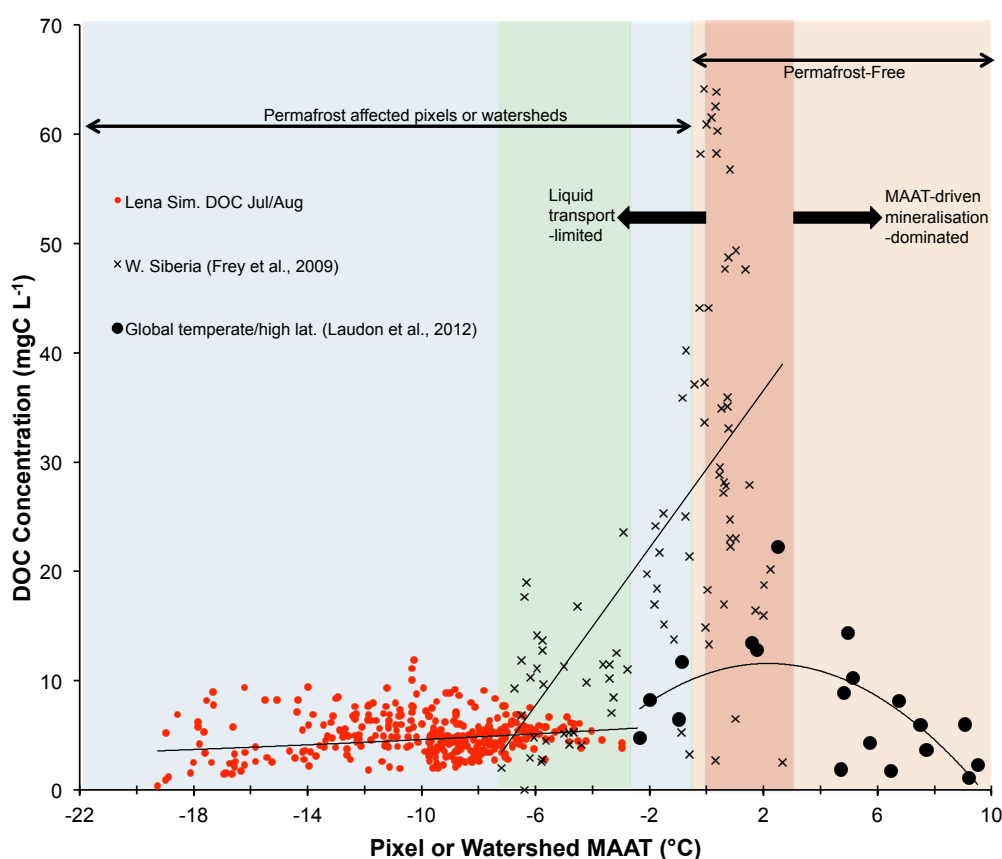787 mainstem of the Kolyma river from Denfeld et al., 2013 are shown inset.
788
789

790
791 **Figure 7:** Mean summertime DOC concentrations (mgC L^{-1}) plotted against mean annual
792 air temperature (MAAT, °Celsius) for simulated pixels over the Lena river basin (red
793 circles), and observations for largely peat-influenced areas in western Siberia as
794 reported in Frey et al., 2009 (black crosses), and observations from a global non-peat
795 temperate and high latitude meta-analysis (black circles) reported in Laudon et al.
796 (2012). The blue region represents permafrost-affected areas, while the orange region
797 represents permafrost-free areas. The green region bounds the area of overlap in MAAT
798 between the observed and simulated datasets. The dark red shaded area corresponds to
799 the MAAT 'zone of optimality' for DOC production and transport proposed by Laudon et

800 al. (2012). Regression curves of DOC against MAAT for each of the separate datasets are
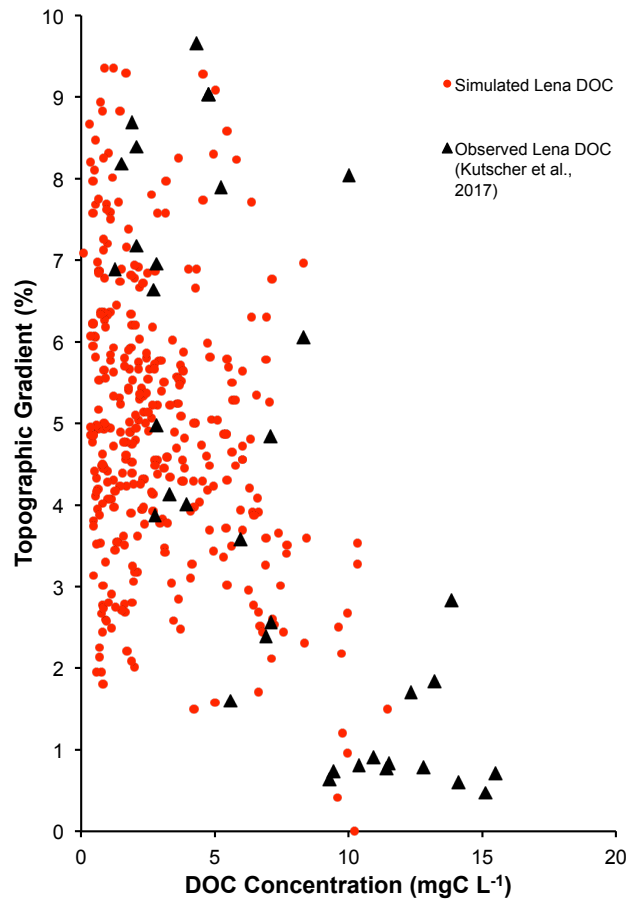801 shown for each individual dataset.
802

803
804 **Figure 8:** Variation of DOC concentrations versus topographic slope in Kutscher et al.,
805 2017 (black triangles) and (red dots) as simulated and averaged for the summer months
806 (JJA) over 1998-2007; observed values were measured during June and July 2012-2013.
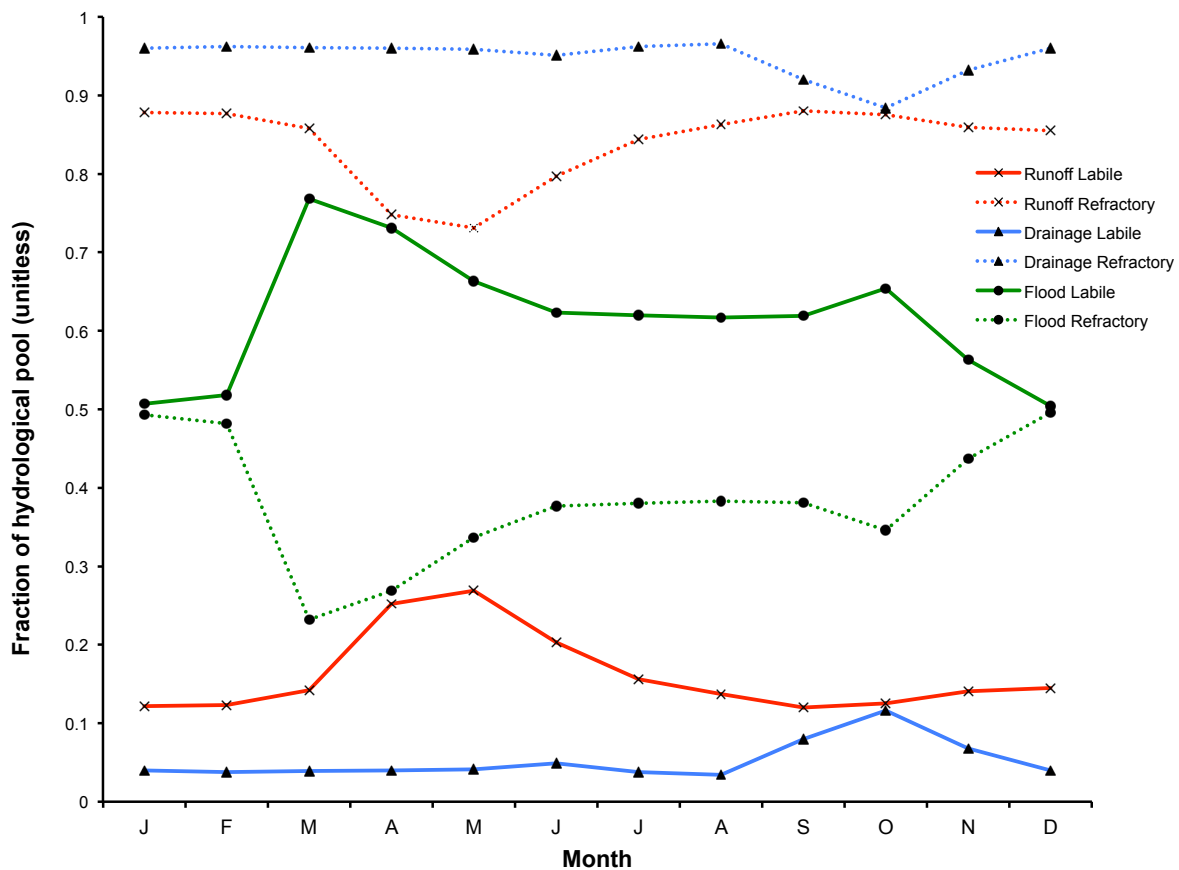807
808 **(a)**
809

810
811
812 **Figure 9:** The mean monthly fraction of each hydrological pool's (runoff, drainage,
813 floodplains) carbon reactivity constituents (labile and refractory) averaged across the
814 simulation area over 1998-2008.
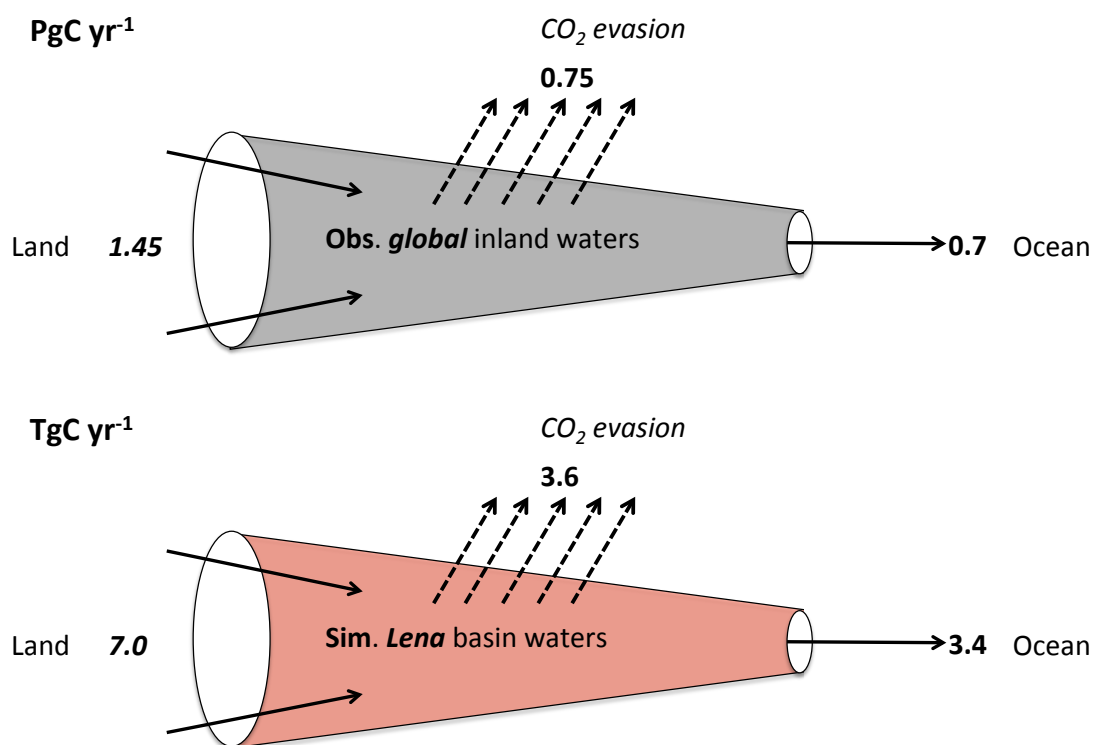815

816

817   **Figure 10**: Simplified 'leaky pipe' diagram representing the transport and processing of
818   DOC within the land-ocean hydrologic continuum. The scheme template is taken from
819   Cole et al. (2007), where we reproduce their global estimate of DOC and non-
820   groundwater discharge portion of this flow in the top panel (PgC yr^{-1}), and the
821   equivalent flows from our Lena basin simulations in TgC yr^{-1} in the bottom panel. Thus
822   easy comparison would look at the relative fluxes within each system and compare them
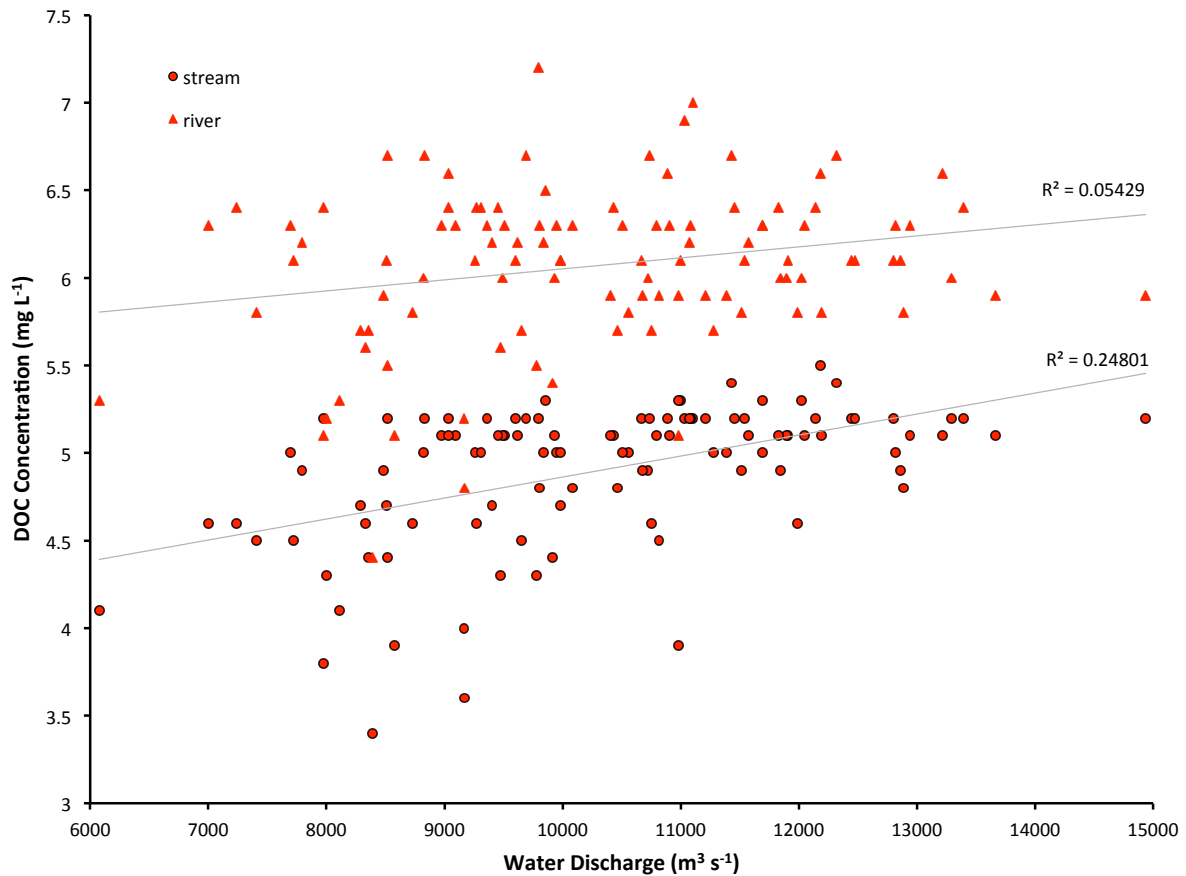823   to the other.
824
825

826
827
828   **Figure 13:** Simulated basin-mean annual DOC concentrations (mg L^{-1}) for the stream
829   and river water pools regressed against mean annual simulated discharge rates (m^3 s^{-1})
830   at Kusur over 1901-2007. Linear regression plots with corresponding R^2 values are
831   shown.
832
833
834